

Multi-band Ambient RF Energy Harvesting Circuit Design for Enabling Battery-less Sensors and IoTs

Ufuk Muncuk, Kubra Alemdar *Student Member, IEEE*, Jayesh D. Sarode, and Kaushik R. Chowdhury, *Senior Member, IEEE*

Abstract—Ambient RF energy harvesting allows powering low-power electronic devices without wires, batteries, and dedicated energy sources. Current RF energy harvesting circuit designs for ambient RF harvesting are optimized and fabricated for a predetermined frequency band. Thus, a single circuit is tuned for a given band with simple extensions to multiple circuits operating individually in distinct bands. Our approach is different in the sense that it designs and implements a common circuit design that can operate on multiple different RF cellular and ISM bands. This paper makes two contributions. First, it presents a study of ambient RF signal strength distribution conducted in Boston city, indicating locations and associated RF bands that can point towards the practicality of ambient RF energy harvesting. Second, it demonstrates an adjustable circuit for harvesting from LTE 700 MHz, GSM 850 MHz, and ISM 900 MHz bands with one single circuit. Our circuit design is fabricated on printed circuit board with comprehensive evaluations at each associated frequency to test the power conversion efficiency. In addition, we characterize the charging performance, and feasibility of powering sensors outdoors such as TI ez430-RF2500. Results reveal more than 45% power conversion efficiency (PCE) for our prototype.

Index Terms—Ambient RF energy harvesting, IoT, adjustable impedance matching, schottky diode, sensor, voltage multiplier

I. INTRODUCTION

WITH recent advancements in low-power integrated circuits and emerging Internet of Things (IoT) applications, ambient energy harvesting has become a promising approach to power widely deployed sensing, computing, and communication devices. This technology raises the possibility of self-sustainable or energy-neutral sensors. It also promises associated cost reduction by elimination of battery replacements and reduces energy-related maintenance downtimes.

In this paper, we focus on ambient RF energy harvesting that aims to convert the power within the RF signals incident at the antenna into functional DC power. Although this technique has the least incident energy availability compared to other alternate energy sources, such as solar and wind, RF energy harvesting (RF-EH) has several unique advantages: It can be used at any location with strong RF signals, especially where sunlight is unavailable, or in indoor spaces equipped with dedicated transmitters. Although ambient RF energy shows some fluctuation on power level, it does not show large scale fluctuation related to the absence (non-existence) of energy source with the time of day and weather conditions, which must be considered in other sources like solar and wind. The form factor of the harvesting circuits can be small, and does not involve moving parts. Also, with intelligently designed

antennas, different user-friendly shapes are possible, like surface plates, wearables etc. These circuits are all electronic and cheap to produce, without considerations of surface dust impacting the efficiency, as is in the case of solar panels.

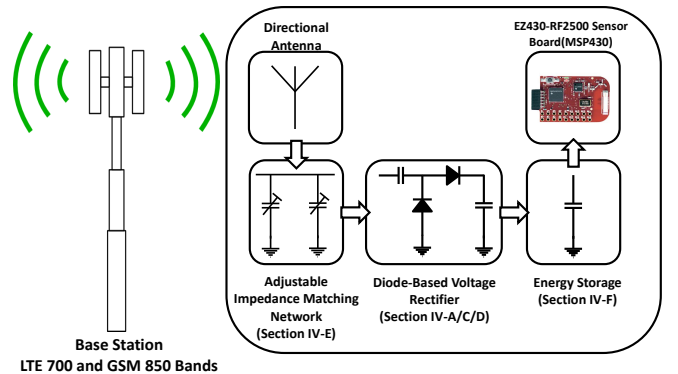


Fig. 1: Overview of our adjustable ambient RF energy harvesting system.

A. Limitation of Existing RF-EH Circuit Solutions

Ambient RF-EH circuits typically operate within a given frequency band when excited by an ambient signal [1]. Multiple such circuits can be arranged in an array, where each harvester is optimized for a specific narrow-band channel with its own impedance matching network [2]. Thus, existing solutions for ambient RF energy harvesting have limited capability in harvesting ambient RF signals from multiple frequency bands. The main reason for this is the preference for simplicity where only one voltage rectifier is connected with a single impedance matching network. This design simplicity results in minimizing cost per sensor and reduces complexity of repair.

For the specific case of ambient RF-EH, the sensor nodes that are interfaced with an energy conversion circuit present a load impedance value depending on its current consumption and operational voltage. Since most existing circuits are typically optimized for a specific load impedance, they are not flexible enough to allow a seamless switch to a different sensor node. At such times, the circuit needs to be modified by adjusting the impedance matching network with the load impedance of new sensor node. This increases the complexity of repair and cost of fabrication, while impacting the generality of interfacing with a large number of different sensors that may typically compose an IoT testbed. In addition, ambient RF energy harvesting enables *battery-free communication* for

IoT applications. Most existing works either focus on only a specific channel, such as a television channel [12]-[15], or use a multiband array composed of multiple antennas tuned to individual channels. While multi-band harvesting increases the output DC power by combining the contributions from the individual circuits, such designs increase complexity and cost of the system [19]. For these reasons, we are motivated in our goal of designing a simple RF-EH circuit design that can power up any sensor mote on a wide range of cellular and unlicensed bands without changes at the circuit level.

B. Research Contributions

Figure 1 shows component blocks of our proposed ambient RF-EH circuit. The voltage rectifier converts the incident RF power into functional DC power. The impedance matching approach in this paper contains a tunable impedance network that allows the circuit to select the excited frequency band according to available ambient power and provides the maximum power delivery from antenna to voltage rectifier for that band. The energy storage ensures smooth DC power delivery.

The main contributions of our work can be summarized as follows:

- We present a systematic study of ambient RF signal strength distributions to create an RF-harvesting map. This map covers both locations and associated RF signal bands in the city of Boston, USA, that demonstrate the extent and practicability of this form of ambient energy harvesting.
- We design a **tunable impedance matching network** composed of off-the-shelf components, such as adjustable capacitors (i.e. trimmers) to adapt the impedance matching network configuration with the selected RF band using a single fabricated ambient RF energy harvesting circuit that makes practical deployments possible by interfacing with any sensor mote.
- We enhance our previously reported ISM band-only harvesting circuit design to cover both cellular and ISM bands. Thus, the circuits presented in this paper show significant design advancement to allow harvesting from LTE 700 MHz, GSM 850 MHz, and ISM 900 MHz bands. This circuit itself is designed and implemented with zero-bias Schottky diode HSMS-285C on a printed circuit board (PCB), and optimized based on the characteristics of ambient signal strength distributions obtained from our survey.
- We undertake comprehensive performance evaluations: In a controlled laboratory setup, we validate the performance of proposed ambient RF-EH circuit for different frequency bands in terms of power conversion efficiency. Second, we characterize the charging performance and show the feasibility of powering a sensor mote in the outdoor environment. Specifically, we demonstrate battery-free communications by interfacing our circuit with Texas Instruments (TI) eZ430-RF2500 sensor motes that operates only by harvesting ambient RF signals at LTE700 and GSM850 bands.

The rest of this paper is organized as follows: In Section II, we describe the related work, followed by discussion on the

survey of signal strength distribution for ambient RF energy harvesting in Section III. The circuit architecture and design challenges are described in Section IV. We undertake the performance evaluation of the fabricated circuit in Section V. Finally, Section VI concludes our work.

II. RELATED WORK

Ambient energy harvesting has attracted from the research community in the recent years. There are various sources of energy from the surrounding environment which are harvestable such as solar, wind and RF energy. In [3], an ultra-wideband(UWB) transceiver is powered with a energy harvesting active networked tags by using solar energy harvesting. Ambient wind energy harvesting are discussed in [4],[5],[6].

A. Dedicated Energy Sources

During the last few years, RF-EH circuits for dedicated and ambient RF sources have made rapid strides. Park *et al.* simulated a *rectenna* design which yields an efficiency of 78% at more than 10 dBm by using a dedicated RF source [7]. In [8], a RF-DC converter with custom antenna design achieved the efficiency of up to 40% for more than -10 dBm for the frequency band between 840 and 975 MHz. Le *et al.* designed CMOS based RF-DC power converter which provides RF sensitivity at -22.6 dBm and obtains 60% efficiency at -8 dBm [9]. This power converter was optimized for far field at which distance is 44 m from 4W EIRP source. However, these existing circuit designs have limited RF power range and frequency bandwidth in which high power conversion efficiency is possible. The dual-stage circuit design in [10] proposed the RF harvesting both in the high input power and the low input power ranges up to -20 dBm.

B. Ambient Energy Sources

Compared to dedicated RF energy sources, ambient RF energy is available from sources such as cellular base stations, WiFi transmitters, satellite communication transceivers, and analog/digital TV transmitters. Pure ambient RF-EH circuit designs can be classified as follows: (i) **a single circuit harvesting energy at a given ambient frequency band**, and (ii) **a harvester array consisting of multiple circuits, each of which is tuned to one specific band with its own impedance matching network**. As a simple extension, the latter configuration provides wide-band harvesting by varying the impedance of the voltage rectifier [11]. Nishimoto *et al.* showed an implementation of sensor node that harvests from TV transmitters [12]. Vyas *et al.* powered an embedded MCU operation using single-tone digital TV band signals at distance of 6.3 km from source. Here, the RF-DC charge pump was designed with a peak efficiency of 20% at input power of -3 dBm [13]. [14] addressed the issue of time-variations of TV signals by developing an algorithm to control the duty-cycle of sensors and mitigating the effects of leakage problem in capacitors. Similarly, [15] utilized digital TV band to power a sensor at 10.4 km from source, with a base transceiver station operating at a center frequency of 738 MHz.

Related Work	RF Source	RF Sensitivity /DC Output Voltage	Peak Conversion Efficiency	Load	Range/Rx Antenna Gain	Matching Architecture	Technology
S. Keyrouz [1]	DTV (470 – 810 MHz)	−15 dBm @ 0.725V	NA	NA	1.24 mi/4.27 dBi	L Matching Network with Lumped elements	HSMS-282C HSMS-285C
A. N. Parks [2]	DTV (539MHz) ISM (915 MHz) 267, 400, 600, 900 and 1350 MHz	−10 dBm	25 - 30% @ −10 dBm 5 - 10% @ −10 dBm	100K Ω	2.61 mi (DTV)/6 dBi 5.5 yd (ISM)/6 dBi NA	L Matching Network with Band pass Filter	HSMS-285C
S. Scorcioni [8]	ISM (868MHz)	−16 dBm @ 2V	58% @ −3 dBm	NA	Indoor Experiment	NA	130nm CMOS
P. Nintanavongsa [10]	ISM (902 – 928 MHz)	−20 dBm @ 1.8V	NA	MICA2	21.87 yd Indoor Experiment	NA	HSMS-2852 HSMS-2822
Z. Liu [11]	GSM900 (915 MHz) GSM1800 (1800 MHz)	−15 dBm	30%	2.1K Ω	NA	Transmission Line	HSMS-2850 ATF34143
H. Nishimoto [12]	DTV (512 – 566 MHz)	−9 dBm	8% @ 10K Ω	TI EZ430	4.1mi/NA	NA	NA
R. J. Vyas [13]	DTV (512 – 566MHz)	−14 dBm (single tone) −37 (multi tone)	19.5% @ 1M Ω	MCU	3.91 mi/7.3 dBi	L Matching Network	NA
R. Shigeta [14]	DTV (512 – 566MHz)	−15 dBm @ 1.1V	7% @ 470K Ω	TI EZ430	3.91 mi/5 dBi	L Matching network	SMS-7630 HSMS-286C
A. N. Parks [15]	DTV (539 MHz) Cellular (738 MHz)	−8.8 dBm (DTV) −18 dBm (Cellular)	23% @ −8.8dBm 26% @ −18 dBm	Sensor Node	6.46 mi(DTV) /6 dBi and 2 dBi 218.7 yd (Cellular) /6 dBi and 2 dBi	NA	Seiko S-882Z IC Charge Pump
Powercast 2110B [17]	ISM (902 – 928 MHz)	−11.5 dBm @ 1.8V	NA	TI EZ430	Indoor Experiment	NA	CMOS
D. Masotti [18]	GSM900 (900 MHz) GSM1800 (1750 MHz) UMTS (2150 MHz) WiFi (2450 MHz)	−10 dBm (GSM900) NA NA −13 dBm (WiFi)	18% @ −10dBm NA NA 10% @ −13 dBm	50 Ω	1.1 yd/NA	Transmission Line	SMS-7630
M. Pinuela [19]	DTV (470 – 610MHz) GSM900 (925 – 960 MHz) GSM1800 (1805 – 1880 MHz) 3G (2110 – 2170 MHz)	−25 dBm (single tone) −29 dBm (multi tone)	40% (end-to-end)	100 μ Capacitor	NA/4.35 dBi(DTV) NA/4.42 dBi(GSM900) NA/4.32 dBi(GSM1800) NA/4.39 dBi(3G)	L Matching network	SMS-7630
M. Stoopman [21]	ISM (915 MHz) and ISM(886 – 908 MHz)	−27 dBm @ 1V	40% @ −17 dBm	1M Ω	1.39 yd /NA 2.19 yd /NA	NA	90nm CMOS
S. Agrawal [22]	Simulation RF Source: 915 MHz Simulation RF Source: 900 MHz Simulation RF Source:945 MHz	−10 dBm @ 1.3V	79% @ −10 dBm 80% @ −10 dBm 75% @ −10 dBm	50K Ω 60K Ω 10K Ω	NA NA NA	L Matching Network with Lumped Elements Pi Matching Network with Lumped Elements Transmission Line (Microstrip)	HSMS-2852
S. D. Assimonis [23]	ISM (868 MHz)	−30 dBm @ 29.3 mV	9% @ 10K Ω	Sensor Node	Indoor Experiment	Transmission Line (Microstrip)	HSMS-285C

TABLE I: Comparative evaluation of state-of-the-art RF energy harvesting circuits and systems.

C. Multi-Energy Sources

Multiband harvesting has been studied in [16] through simulations with three individual impedance matching circuits, each tuned to separate frequency bands. Since ambient power typically has low levels, it requires highly efficient *rectennas* that operate within a single narrow band. Hence, harvesting energy from multiple frequency bands simultaneously is critical to ensure reliable operation [18]-[19]. In existing works, multiband array with multiple antennas tuned to individual bands have been designed *rectennas*. The signals are then combined to provide an overall output DC power that is the summation of DC output from each of them. A multiband rectifier with a wideband antenna, instead of multiple antennas, and a summation network is described in [20] that enables combining power from these rectifiers, even if all bands are not available at the same time at a given location.

Table I summarizes the performance of various circuit designs in terms of achieved efficiency versus RF power source, frequency, RF sensitivity, nonlinear component technology, and impedance matching architecture. It indicates that circuit designs with CMOS technology allow lower minimum RF input power, but diode based designs using HSMS technology are comparatively more efficient.

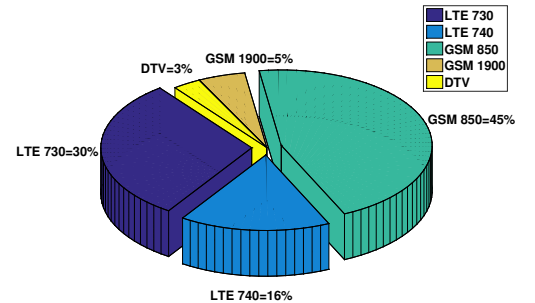


Fig. 2: Percentage times that a given channel contains the highest RF energy measured at Boston subway stations.

III. SPATIO-TEMPORAL AND MULTI-FREQUENCY RF-EH STUDY IN BOSTON CITY

To determine the frequency bands and sensitivity of ambient RF-EH, we conducted an RF spectrum study between 0.3 and 3 GHz. This study provides an early insight into characterizing the energy availability in actual city locations. The key take-away message here is: there is no one RF band that provide the highest RF-EH capability city-wide; instead identifying the set of top performing bands plays a critical role in designing

Index Name	Location Description	Experimental Time-line	Frequency Band	μ (dBm)	σ (μ)
MFA-1	Museum of Fine Arts; outdoor	July 26, 2016 - July. 30, 2016 (Noon)	LTE (734 MHz – 756 MHz)	-6.7	1.818
MFA-2	Museum of Fine Arts; outdoor	Aug. 1, 2016 - Aug. 5, 2016 (Noon)	GSM (869 MHz – 894 MHz)	-6.9	2.017
Eli Hall-1	Northeastern University, Krentzman Quadrangle; outdoor	July 26, 2016 - July. 30, 2016 (Early Morning)	LTE (734 MHz – 756 MHz)	-8.7	0.284
Eli Hall-2	Northeastern University, Krentzman Quadrangle; outdoor	Aug. 1, 2016 - Aug. 5, 2016 (Early Morning)	GSM (869 MHz – 894 MHz)	-4.5	0.286
Symphony-1	Symphony Hall; outdoor	Aug. 3, 2016 - Aug. 7, 2016 (Morning)	LTE (734 MHz – 756 MHz)	-7.5	0.959
Symphony-2	Symphony Hall; outdoor	Aug. 8, 2016 - Aug. 12, 2016 (Morning)	GSM (869 MHz – 894 MHz)	-6.7	0.883
Prudential-1	Prudential Tower; outdoor	Aug. 8, 2016 - Aug. 12, 2016 (Afternoon)	LTE (734 MHz – 756 MHz)	-18.3	1.308
Prudential-2	Prudential Tower; outdoor	Aug. 12, 2016 - Aug. 14, 2016 (Afternoon)	GSM (869 MHz – 894 MHz)	-13.3	0.851
Arlington-1	Arlington, near the subway station; outdoor	Aug. 15, 2016 - Aug. 19, 2016 (Afternoon)	LTE (734 MHz – 756 MHz)	-22.1	0.468
Arlington-2	Arlington, near the subway station; outdoor	Aug. 15, 2016 - Aug. 19, 2016 (Afternoon)	GSM (869 MHz – 894 MHz)	-24.7	0.338
Boston Common-1	Boston Common Public Park; outdoor	Aug. 16, 2016 - Aug. 20, 2016 (Evening)	LTE (734 MHz – 756 MHz)	-8.3	0.21
Boston Common-2	Boston Common Public Park; outdoor	Aug. 16, 2016 - Aug. 20, 2016 (Evening)	GSM (869 MHz – 894 MHz)	-5.5	0.143

TABLE II: Summary of ambient RF power experimental setups.

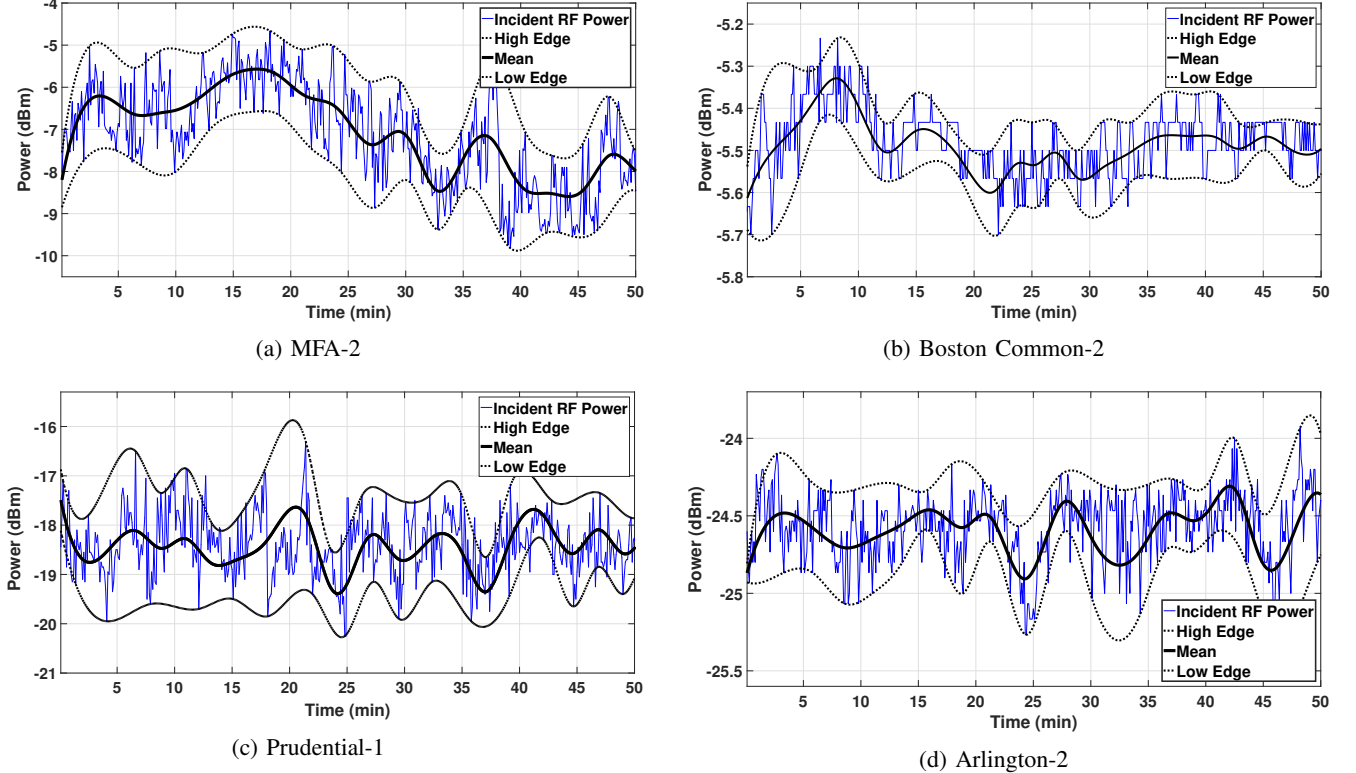


Fig. 3: Comparison of ambient RF energy profiles at four locations in Boston in terms of incident RF power.

our circuit.

Our study was conducted in the GSM850, GSM1900, LTE730, LTE740, and DTV bands within Boston, USA. Measurements for available ambient RF power at each frequency band were collected from outside of 40 subway stations at the street level, to ensure the sample locations were well distributed. We found that the percentages of each ambient RF signal band where the highest power is measured is composed of 46%, 5%, 30%, 16% and 3% for GSM850, GSM1900, LTE730, LTE740, and DTV, respectively as a fraction of all sample locations, as seen in Figure 2. This implies that 92% available ambient RF power locations are served by LTE700 and GSM850 bands.

We then measured the available ambient RF power in the LTE700 and GSM850 bands in six different locations, such as within the university, museum, shopping center, subway station entrance, park and concert theater, within Boston city.

These particular locations were selected to help us analyze the impacts of geographical terrain, structural distribution and density on RF energy levels in the outdoor environment. Table II gives a summary of our RF measurement survey features, including locations, time, frequency bands, and mean(μ) and standard deviation(σ (μ)) of measured powers. The measurement samples were obtained in 50-minute collection windows at each location. Each such trial was repeated at the same time and location for 5 days in order to investigate the environmental effect on harvested ambient energy. We used our preliminary energy harvesting circuit [10] with a 50-ohm LP0410 Log Periodic PBC antenna manufactured by Ettus Research LLC [29], and Sinometer VA18B Multimeter with RS232 USB Cable and Laptop in order to record the instantaneous output voltage of the energy harvester. To estimate the exact incident ambient RF power signals, we first create an RF power mapping table between output voltage and input

Index Name	R_b	R_a	Mean of Building Height in R_b (ft)	Mean of Building Height in R_a (ft)	Average Height per grid in R_b (ft/grid)	Average Height per grid in R_a (ft/grid)	μ (dBm)	$\sigma(\mu)$
MFA	965	380	55.8	54.8	3.87	6.94	-6.7	2.017
Prudential	907	350	60.1	100.2	16.15	44.27	-18.3	1.308
Arlington	625	265	82.34	72.1	19.12	19.6	-24.7	0.338
Boston Common	1418	689	55.1	46.32	18.88	2.1	-5.5	0.143

TABLE III: Statistical information of building height at corresponding locations.

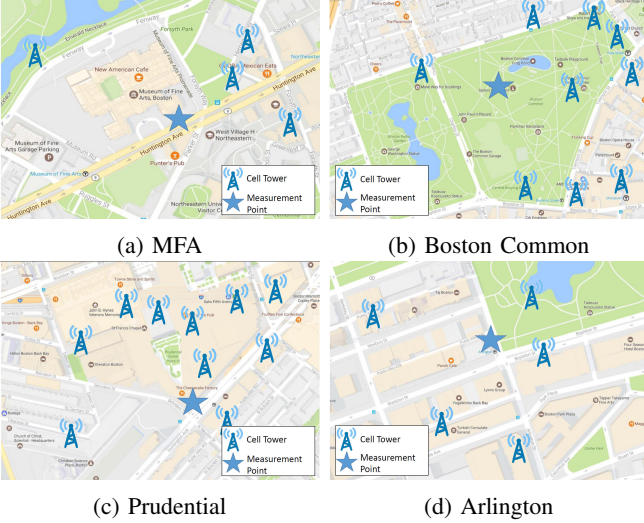


Fig. 4: Geographical maps of our outdoor experiments at four locations with their associated base-stations.

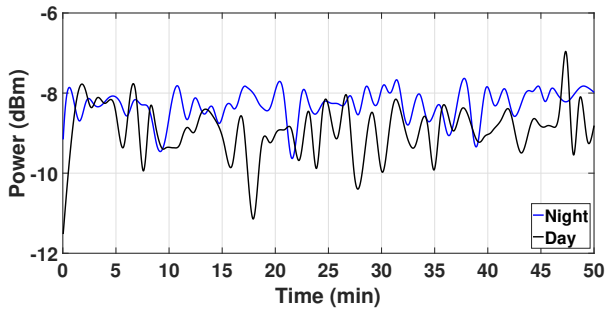


Fig. 5: Levels of average RF power at subway stations, universities, museums, shopping centers, parks in Boston city.

power using Agilent N5181 MXG RF signal generator and Agilent E5061B vector network analyzer in a lab environment. Accordingly, the available ambient RF power can be estimated by comparing the instant output voltage value of energy harvesting circuit recorded by multimeter. Figure 3 shows the energy profiles for 4 locations from our measurements, and Figure 4 depicts their associated setup maps with surrounding base stations. In order to generate the energy profile of each location, we computed the average signal of all 50-minute experimental data sets for the same day, as well as computed the signal envelop to visualize the upper and lower bounds in the signal. In order to demonstrate the correlation of the geographical location to the trends seen in the received power plots, we divide the experimental area into grids of $5 \times 5 \text{ ft}^2$. The overall area of interest is identified by determining the

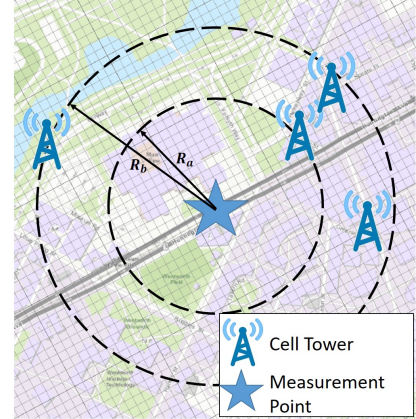


Fig. 6: Different effective reception areas according to proximity range of cell towers; R_a and R_b represent the radius of reception areas from experimental setup point to the nearest and farthest cell tower, respectively.

radius of an effective reception area given the proximity range of surrounding cell towers, as shown in Figure 6. We study the correlation between the average building heights within the area being study and the incident RF signal. We calculated the mean of building height in the effective reception area contained with concentric circles of radii R_a and R_b and the average building height per grid square as seen in Table III. We use the building footprint dataset of the city of Boston and statistical tools from the ARCGIS software for each experimental location. We note that each signal has a different standard deviation based arising from short-term fluctuations in the received signal. For example, *MFA-2* shows high variation in the GSM850 frequency band, even though the source base station's is situated close to the receiving sensors. This is because, as shown in the topographical map in Figure 4a, the average building height is comparatively large at R_a is 6.94 ft/grid. As opposed to this area, *Common-2* is located within an open space with a smooth trend in the received signal, which also correlates with the comparatively low 2.1 ft/grid of average building height. Although the distance between the measurement point and the closest cell tower at *Boston Common* is greater than other locations (i.e *MFA*), more incident RF power is obtained at *Boston Common* due to reduced average building height in radius of R_a . Furthermore, we observe that while the density of base stations around *Prudential-1* (amidst other high-rises) is higher compared to *Boston Common* (open field) and *MFA* (low-height buildings), the average ambient RF power is lower as -18.3 dBm/s . This occurs because of physical obstructions in the path (e.g multi-

path fading, attenuation from buildings, reflections, see Table III). Moreover, for measurements taken in the rush-hours of the day, *MFA* exhibits more fluctuations than other locations since there are large number of moving signal reflectors on the road. In addition, we conducted night-time experiments at the locations with high signal levels, such as *MFA*, *Symphony* and *Boston Common*, to contrast the variation of available power between night and day time. Figure 5 gives an example result from *Symphony* by comparing the average ambient RF power of both night and day time. The variations in the RF power observed at night, with $0.528\sigma(\mu)$, is less than that during the day, with $0.92\sigma(\mu)$. This trend is expected as the number of moving signal reflectors decreases at night. The drop in the average ambient RF power from -7.9 dBm from the day to -8.2 dBm at night is partly due to reduced mobile traffic that also influences the energy profile of the cellular transmitters.

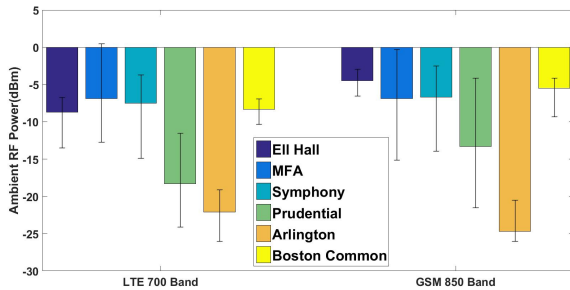


Fig. 7: Levels of average RF power at subway stations, universities, museums, shopping centers, parks in Boston city.

Finally, Figure 7 summarizes average ambient RF power levels for LTE and GSM frequencies over a set of locations with maximum and minimum values. This influences our design goal to create RF-EH circuits that are responsive in a power range between -25 and 0 dBm with high efficiency.

IV. RF-EH CIRCUIT DESIGN AND IMPLEMENTATION

The ambient RF-EH circuit demonstrated in this paper is composed of a Dickson diode-based voltage rectifier circuit with a parallel configuration of capacitors in each stage that makes the impedance matching less complex. We further show a novel adjustable impedance network matching, and also the effect of its selection on the energy storage. First, we explain how to select the components of each sub-part of the circuit according to the performance constraints, and also how each of the components influence the performance of the overall circuit.

A. Diode Selection

The key challenge in designing an ambient RF-EH circuit is the need to operate with low power RF signals. As seen in Figure 7, the average power amplitude of ambient RF signals can be as low as -25 dBm (see Section III), which means the amplitude of the received signal power is less than $3.2\mu\text{W}$. This generates 4 mV RMS and 5.7 mV peak AC voltage for a typical $50\ \Omega$ antenna. In general, the threshold voltage

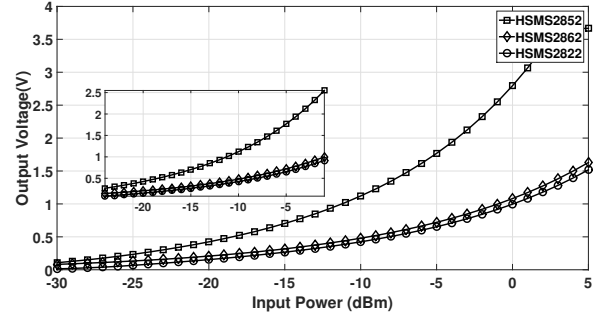


Fig. 8: The effect of diodes on output voltage of ambient RF-EH circuit.(The performance of chosen set of Schottky diode with power range measured during Boston RF study)

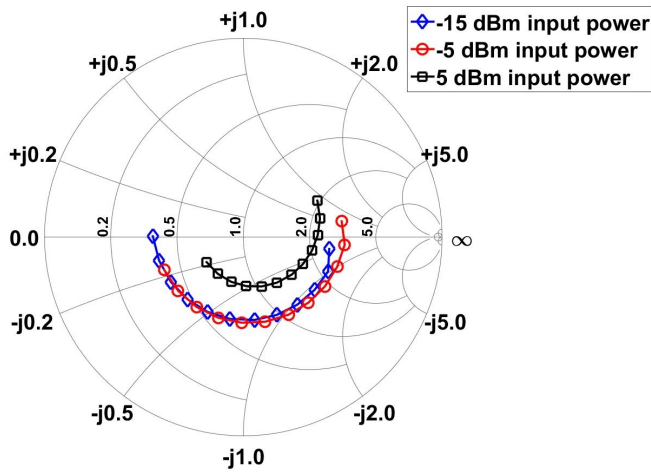
of typical diodes is much higher than the peak voltage of the ambient RF signal at -25 dBm. Therefore, the diode chosen for the RF-EH circuit should have the least possible turn-on threshold voltage. Furthermore, these diode must have faster switching time compared to a traditional diodes since ambient RF-EH occurs at high frequencies. For these reasons we selected Schottky diodes for our ambient RF-EH circuit designs.

Schottky diodes contain a fast metal-semiconductor junction with a forward voltage drop of less than 0.15V compared to a semiconductor-semiconductor junction [24]. Figure 8 depicts the effect of diodes on the output voltage of an ambient RF-EH circuit. As a candidate set, we included Schottky diodes from Avago Technologies, such as HSMS-2822, HSMS-2852, and HSMS-2862, which have the turn-on voltages of 340 mV, 150 mV, and 350mV measured at 1 and 0.1 mA, respectively. We used Agilent Advance Design System (ADS) with one-stage Dickson rectifier and parameter sweep of -20 to 5 dBm of the input RF power. We focused on analyzing the performance characteristics of these diodes at mostly low input power. However, it is noteworthy that it is feasible to efficiently perform at higher input powers as well. We observed that HSMS-2852 Schottky diode performs much better than HSMS-2822, and HSMS-2862 at the desired input power ranges found during the RF survey. Thus, we employ HSMS-285C in our design that has the same specifications of HSMS-2852, such as the turn-on voltage of 150mV measured at 0.1mA , but comes in a smaller package size.

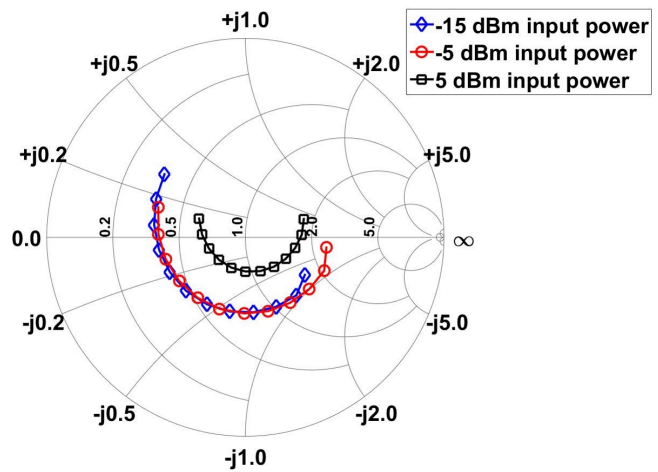
B. Input Power-aware Impedance Matching

Due to the nonlinear characteristic of the diode, the circuit itself exhibits nonlinearity. Thus, the impedance of the ambient RF-EH circuit varies as a function of the amount of power received from the antenna [10]. This necessitates impedance matching with the antenna at a given input power regime to provide the maximum harvesting. Figures 9a and 9b show the effect of RF input powers on the impedance of the ambient RF-EH circuit at LTE 700MHz frequency band that is optimized at -15 dBm and 0 dBm, respectively, when the input power varies from -15 to 5 dBm.

We observe from Figure 10 that the circuit optimized at -15 dBm gives more output voltage than the circuit optimized at



(a) The impedance of the ambient RF-EH circuit (Optimized @ -15 dBm).



(b) The impedance of the ambient RF-EH circuit (Optimized @ 0 dBm)

Fig. 9: Effect of RF input power on the impedance of the ambient RF-EH circuit (Optimized @ 0 dBm)

0 dBm for input powers between -20 dBm and -5 dBm. In addition, the circuit that is optimized at 0 dBm performs much better the circuit optimized at -15 dBm for input powers between -5 dBm and 5 dBm. This implies that impedance matching should be performed according to RF input powers. According to our city-wide RF study, the average input power amplitude is less than -5 dBm. Hence, our design goal in impedance matching is to ensure that the circuit operates optimally around -15 dBm input power level.

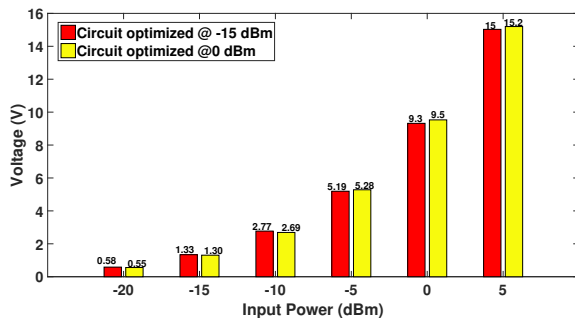


Fig. 10: Effect of RF input power on output voltage of the ambient RF-EH circuit.

C. Selecting the Number of Rectifier Stages

The major design parameter that directly affects the output voltage of the ambient RF-EH circuit is the number of rectifier (multiplier) stages that connected in series. Each stage is a modified voltage rectifier.

Figures 11 and 12 show the impact of number of stages on the efficiency of circuit at LTE 700 MHz band, and GSM 850 MHz band, respectively. We have used Agilent ADS with sweeping input powers from -30 to 20 dBm and varying circuit stages from 1 to 6 . The circuit being simulated is a modified voltage multiplier of HSMS-285C, and the circuit

with each stage configuration is impedance-matched at the desired frequency band. The load value is $81.5K\Omega$, which is chosen for representing the impedance value of sensor mote in a real application.

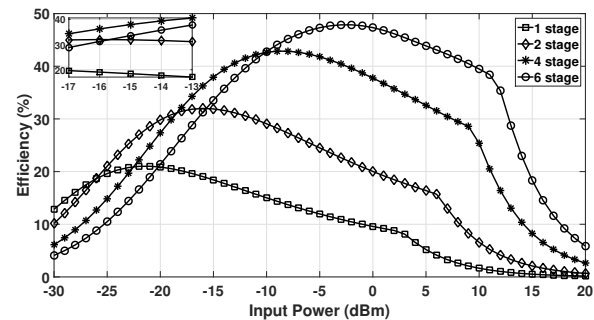


Fig. 11: Effect of number of stages on the efficiency of energy harvesting circuit at LTE band.

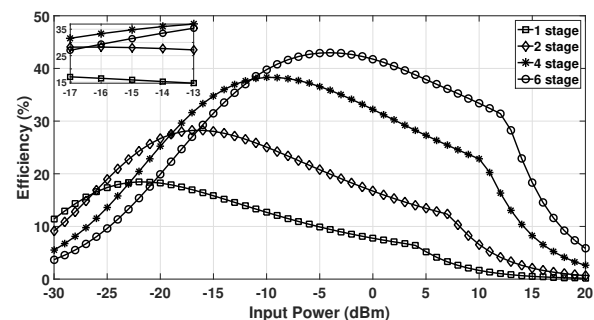


Fig. 12: Effect of number of stages on the efficiency of energy harvesting circuit at GSM band.

We see that the efficiency is not simply higher at a desired input power as the number of stages increases. The increment on number of stages also causes shift on the peak of efficiency

curve towards high powers. This implies that the RF-EH circuit for ambient harvesting applications in low power regimes does not need more number of stages to improve on efficiency. For e.g., the circuit with four stages obtains much higher efficiency between -17 and -13 dBm input RF powers as opposed to the circuits with other number of stages. Hence, we use the rectifier configuration with four stages as the circuit configuration of choice in our design optimization.

D. Effect of Load Impedance on Performance of Ambient RF-EH Circuit

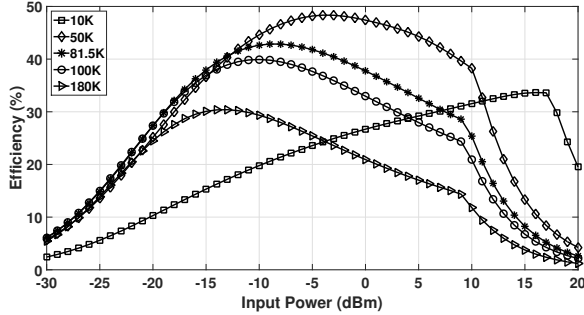


Fig. 13: Effect of load impedance on the efficiency of RF-EH circuit at LTE band.

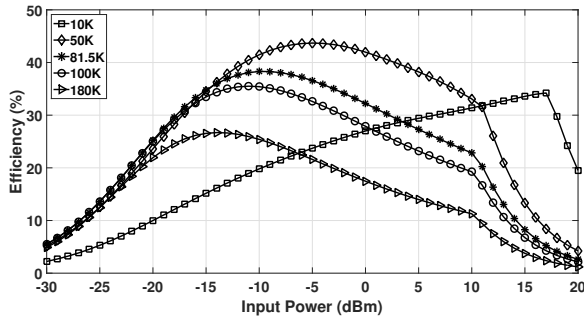


Fig. 14: Effect of load impedance on the efficiency of RF-EH circuit at GSM band.

The load impedance should be selected carefully because it is directly related to impedance matching with the antenna, and has bearing on maximum energy transfer. We simulate the effect of load impedance on the efficiency of the energy harvesting circuit using Agilent ADS with parameters sweeping between -30 and 20 dBm and $10 - 180K\Omega$ for input RF power and load value, respectively. The circuit is 4-stage, impedance-matched for each load configuration, and each stage is a modified voltage rectifier of HSMS-285C. We see from Figure 13 and 14 that the optimal efficiency is attained at a particular load value, and the performance dramatically drops if the selected load is too low or too high.

The electric current consumption of a sensor mote changes with its operation, such as active, sleep, and deep-sleep states. This means that the impedance of the sensor is changing with status of its state. In order to set the correct impedance of the sensor driven by RF-EH circuit, we use the voltage and current

consumption numbers of the sensor in the deep sleep state, where the RF-EH circuit harvests energy without interruption. We use TI eZ430-RF2500 sensor mote which consume $20 \mu A$ in sleep state and $44.4 \mu A$ in active state of at $3.0 V$, which translates to $81.5 K\Omega$ and $180 K\Omega$ resistive load, respectively. These impedance values are used as load value of RF-EH circuit in design, optimization, and fabrication.

E. Impedance Matching Network Design

A key design goal of the ambient RF-EH circuit is to ensure efficient and dissipation-less energy transfer between the antenna and the rectifier circuit. The impedance of the rectifier circuit alters design parameters that directly affect the circuit performance, such as non-linearity of diode used in the rectifier, RF power incident at the antenna, load impedance, and the number of rectifier stage as mentioned in previous sections. Due to this, a well-designed impedance matching network can improve the circuit performance by enabling highly efficient energy transfer between rectifier and antenna with a choice of appropriate matching topology and values of components. Lumped or distributed elements such as resistor, inductor, capacitor and microstrip transmission lines can be used as the component of matching networks [22].

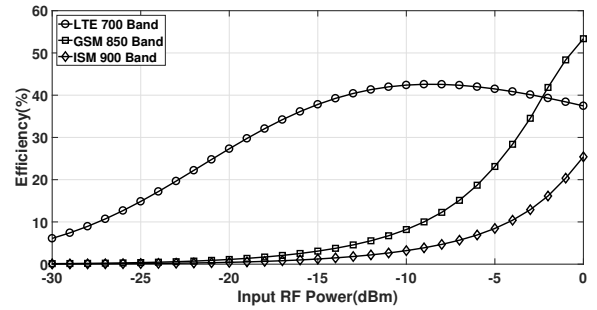


Fig. 15: Efficiency performance of optimized the energy harvesting circuit for LTE band with lumped element impedance matching network optimized in the LTE 700, GSM850, and ISM900 band.

The conventional impedance matching network comprised of lumped or distributed elements perform best with a fixed specific operating condition such as frequency, input power level and load impedance. Any minor change in operating condition impacts the energy conversion efficiency of RF-EH circuit. Figure 15 shows such behavior, where an impedance matching network with lumped or distributed elements does not perform well at different frequency ranges. In the case of ambient RF signals, such digital/analog TV and cellular signals, the range of frequencies is wide. Fabricating more than one circuit that are tuned individually for distinct frequency bands does not allow addition of new bands or change of bands after fabrication. It also lacks adaptability to changes in the RF input powers, which we have empirically observed. To address these issues, we propose a novel impedance matching network that is adjustable and supports the harvesting circuit over LTE 700, GSM 850, and ISM 900 bands. This adjustable configuration of the impedance matching network allows free

choice of any antenna with different characteristic impedances, interfacing between antenna and rectifier, and any type of low-power sensor mote is a viable load for the system. This means that the proposed impedance matching network configuration allows the voltage rectifier to be independent on the impedance of both antenna and load.

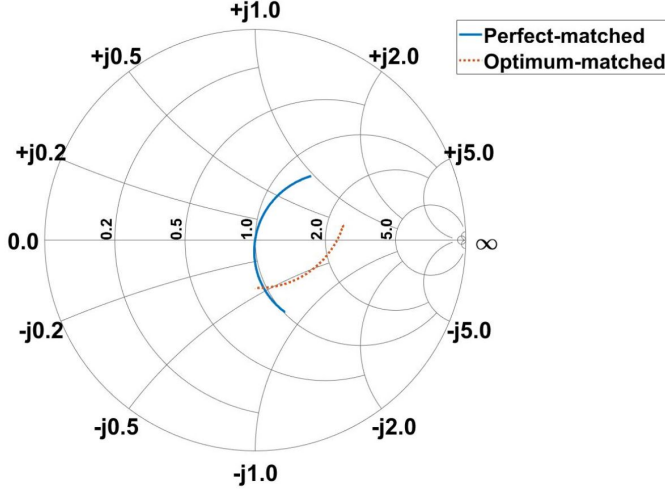


Fig. 16: The impedance of the ambient RF-EH circuit (Optimized @ -15 dBm).

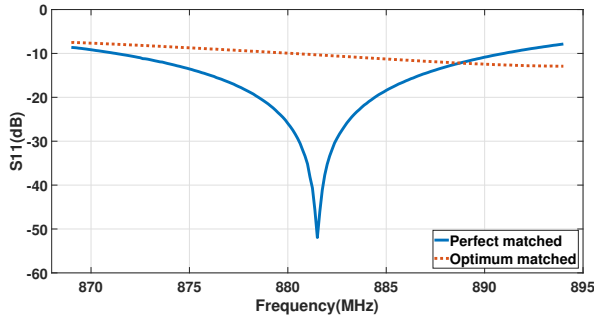


Fig. 17: Measured closed circuit S11 parameters of the ambient RF harvester (Optimized @ -15 dBm).

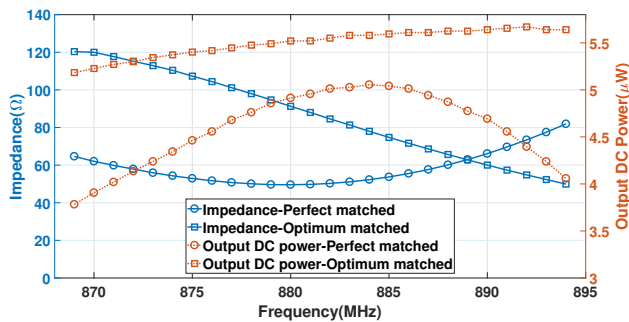


Fig. 18: The effect of impedance matching status on output DC power of ambient RF-EH circuit over GSM 850 band (Input RF power level is -15 dBm).

As a starting point, we attempt to answer a fundamental question: "Is the maximum power delivered to rectifier in the

circuit when the circuit is matched with antenna perfectly?". Figure 16 and 17 show the (i) Smith chart of circuits matched perfectly and optimally, and (ii) reflection coefficient (S11 parameter) performance of these circuits at GSM850 frequency band, respectively. We use four-stage RF-EH circuit interfacing a resistive load of 81.5 K Ω . It is important to note that the measurements are experimentally done using Agilent E5061B vector network analyzer in order to demonstrate the proof of concept. The entire 25 MHz bandwidth within a GSM850 frequency band (869.2 MHz – 893.8 MHz) is studied with an observed reflection coefficient less than -10 dB in the case of perfect-matched network (maximum reflection coefficient with -52 dB at 881.5 MHz). A reflection coefficient within a range -9 dB and -13 dB is seen where impedance values are in close region to center of the Smith chart. Hence, the maximum power transfer between the antenna and the rectifier is expected with large absolute values of S11 (i.e.: $> |10|$ dB) as seen in Figure 17, when the circuit is perfectly matched. However, the comparison of the output power as a function of frequency measured from the output load of the rectifier in two different conditions, as aforementioned above, shows that the rectifier delivers more DC power to the output when it has a slight mismatch with the optimal impedance (see Figure 18). This figure shows the magnitude of the input impedance in y-left axis and the output DC power in y-right axis as a function of frequency within GSM850 frequency band. It is clear from the solid plots that the output DC power measured from perfectly-matched rectifier forms a mountain curve by corresponding to input impedance values with the maximum output power at around 50 Ω . This distribution of the power over frequency band indicates that the desirable region for the highest power is restricted to the close proximity of the center frequency. The impedance values for an optimally matched circuit is not close to 50 Ω , but also it doesn't show any significant changes of power level so that we obtain high output DC power over whole GSM850 band. This is because the impedance matching network tuned the center frequency for perfectly matching the circuit impedance with the antenna can cause more return loss at the frequencies that are progressively away from the center. As different channels are present in a cellular frequency band (i.e. GSM channel numbers: 128–251), the energy harvesting device cannot harvest enough from several channels when it is tuned to a single frequency. As a result, we focused on designing an impedance matching network which can be tuned to a whole individual frequency band rather than just the center frequency of the same band.

In order to get optimal impedance matching with antenna impedance (50Ω), for each determined frequency band, we keep the input RF power fixed at -15 dBm and observe the resulting changes on the output DC power while trimming two shunt trimmer capacitors of the impedance matching network. Figure 19 shows our strategies of tuning: We first compare the output DC power of the RF-EH circuit with the unmatched circuit. Thereafter, we trim the first shunt capacitor ($C1$) and observe how much the output DC power changes with the change in the value of $C1$. When we identify the peak DC power at the output of the RF-EH circuit, we repeat the same

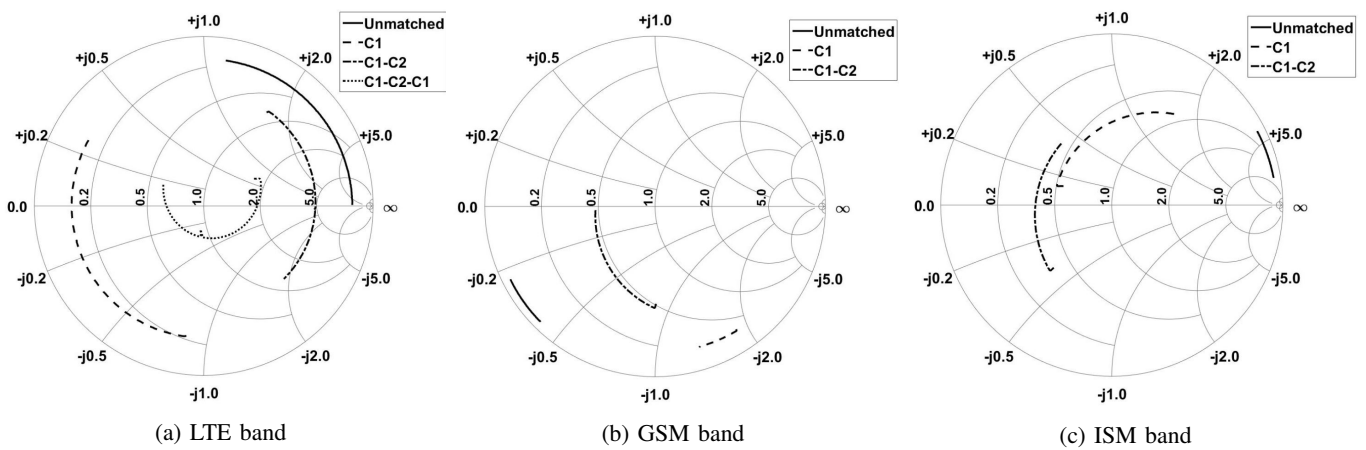


Fig. 19: The strategies of tuning the proposed impedance matching network at the determined frequency bands

procedure to find the value of the second shunt trimmer ($C2$). These iterations finally result in the peak output DC power voltage being attained with the optimal configuration of $C1$ and $C2$. During the matching process, we use Agilent E5061B vector network analyzer to see the change in impedance value of circuit and Sinometer VA18B Multimeter to measure the DC power on the resistive load representing the impedance of sensor mote.

Figure 20 shows the impedance and output DC power of an optimal-matched ambient RF-EH circuit over the determined frequency bands for different input power levels. The circuit optimized with optimal impedance matching shows the same performance behavior explained above over the entire band for each input RF power. This implies that the ambient RF-EH circuit is able to harvest energy from different channels of the cellular band in an efficient way. The proposed impedance matching network performs perfectly for each ambient signal frequency band.

F. Capacitor/Energy Storage Selection

Since available ambient RF power in the environment is insufficient to directly power up low-power devices, harvested energy must be first stored in a capacitor. In order to use store energy efficiently, we recognize that a sensor operates in multiple different states: start-up mode, active mode, and sleep mode. These states require distinct power consumption levels. Since we choose the TI eZ430–RF2500 sensor mote, it requires $376 \mu\text{J}$ at 3.6 V of harvested voltage to turn on the mote for initialization of the μC MSP430F2274 and data communication. The total required energy consumption during one completed operation cycle is $448 \mu\text{J}$, including duration time for each mode in duty cycling mechanism. The required minimum capacitance value (C_{min}) to maintain the sensor node in a perpetual cycle between active mode and sleep mode is:

$$C_{min} = \frac{2E_{con}}{V_{cap}^2 - V_{th}^2} \quad (1)$$

Here, the threshold voltage of capacitor (V_{th}) is 1.8 V and the capacitor voltage (V_{cap}) is 3.6 V . The capacitor voltage

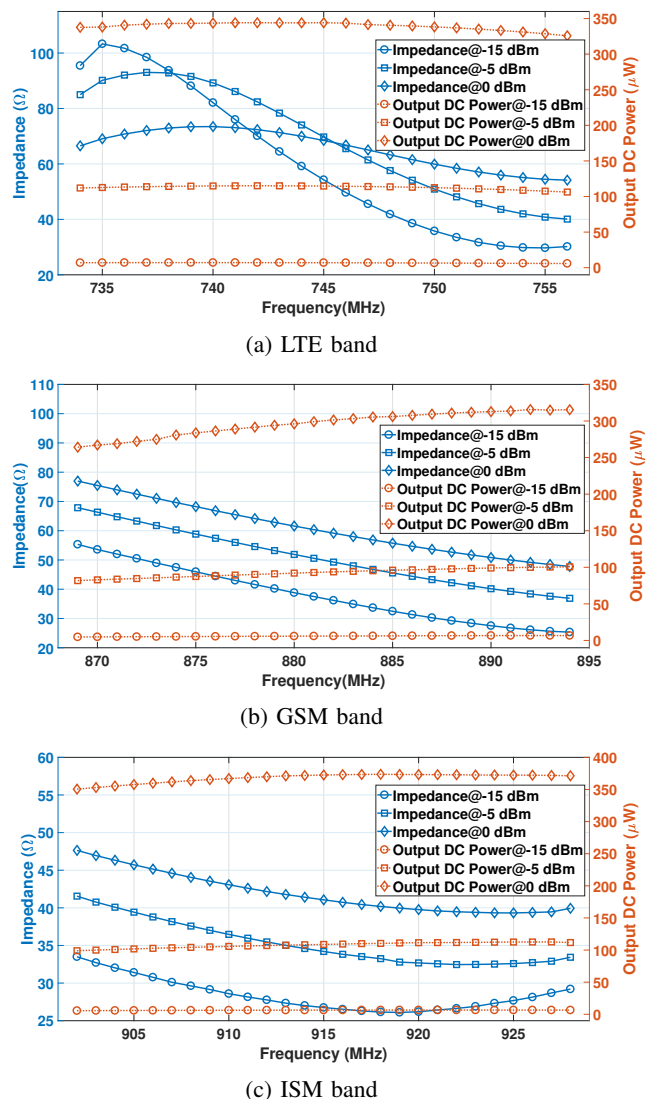


Fig. 20: Impedance and output DC power of the optimal-matched ambient RF-EH circuit over the determined frequency bands.

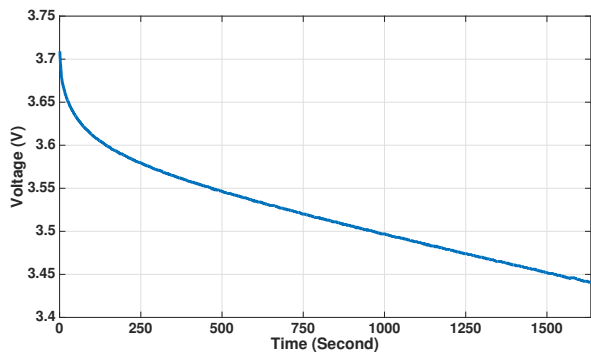


Fig. 21: Self-discharge behavior of the selected storage capacitor.

should be 3.6 V so that the sensor turns on by itself at the start and also V_{th} prevents the sensor from turning itself off after initialization. In these conditions, capacitor value should be greater than approx. $93 \mu\text{F}$ given the energy consumption of the sensor (E_{con}). We now select a MLCC capacitor with a large capacitance value of $3300 \mu\text{F}$ and self-discharge behavior as seen in Figure 21, after verifying it with repeated outdoor experiments. We note that a small capacitance leads to significant reduction in the discharge times. In particular, considering the results of city-wide RF study given in Section III, it is difficult to power up the sensor node because of short-term fluctuation in power levels as seen in Figure 3a compared to [14] that studied TV broadcast channels.

G. Fabrication and Optimization

Figure 22 shows the fabricated PCB of our ambient RF-EH circuit prototype based on performance discussions in Section IV. We design the PCB board as two layers, one of which serves as a ground plane and fabricate the PCB board with FR-4 epoxy glass substrate. Its specifications are shown in Table IV.

Component	Value
Size	2" x 1.5"
Laminate thickness	62 mil FR-4
Number of Layers	2-layer, one serves as a ground plane
Copper thickness	1.7 mil
Trace width	20 mil
Dielectric constant	4.6
Through-hole size	15 mil

TABLE IV: Parameters in PCB fabrication for ambient RF energy harvesting circuit design.

Our prototype follows the design from Section IV. It uses 4-stage Dickson voltage rectifier, in which each stage consists of a HSMS-285C Schottky diode and two stage capacitors and is connected to a 6dBi wideband log-periodic antenna manufactured by Ettus Research LLC. The value of stage capacitor does not have any effect on the output voltage of rectifier but it can affect the responsive time of circuit. We select 100 pF MLCC SMD capacitor as stage capacitor [27]. In order to optimize the impedance matching network, we trim the adjustable capacitors by using Agilent E5061B vector network

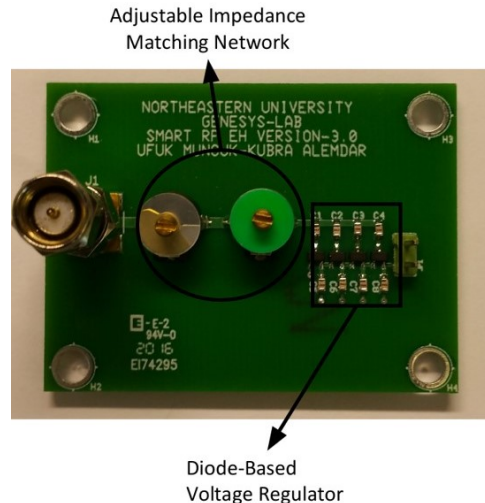


Fig. 22: Prototype of our adjustable ambient RF-EH circuit.

analyzer for the determined ambient frequency range and RF input power level. In particular, our prototype is tuned to the ambient signal frequency bands in LTE 700(734 – 756MHz), GSM 850(869 – 894MHz), and ISM 900(902 – 928MHz). The configurations are summarized in Table V.

Circuitry	Topology	Component	Value
Rectifier	Dickson diode-based Four Stage	Diode Stage Capacitor	HSMS-285C 100 pF
Impedance Matching Network	Adjustable-configured Modified π network	Shunt Trimmer 1 Shunt Trimmer 2	$2.2 - 22 \text{ pF}$ $3 - 36 \text{ pF}$
Energy Storage	NA	Capacitor	$3300 \mu\text{F}$

TABLE V: Fabrication components of our ambient RF energy harvesting circuit.

V. PERFORMANCE EVALUATION

In this section, we study the performance of our circuit using power conversion efficiency (PCE) and charging performance metrics through both indoor and outdoor experiments. Further, we demonstrate battery-free communications using our adjustable circuit and ambient RF signals.

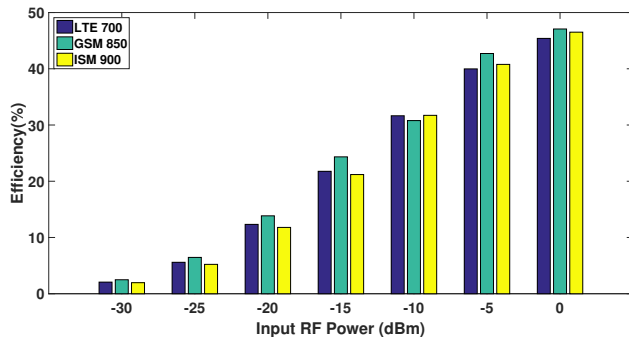
A. Indoor Experimental Study

In the first set of experiments, we examine the PCE in an indoor environment. The circuit is tuned to each target frequency band while using Agilent E5061B vector network analyzer. We use the network analyzer as an RF signal generator to measure DC power output from our prototype by providing RF power from -30 to 0 dBm . We calculate the DC power from measured voltage associated with resistive loads of $81\text{K}\Omega$ and $100\text{K}\Omega$ with Equation 2. The load values are chosen based on the discussions in Section IV-D. We use Sinometer VA18B Multimeter to measure the voltage on the resistive loads. The power conversion efficiency is obtained by using Equation 3 where P_{DC} is the output DC power that is

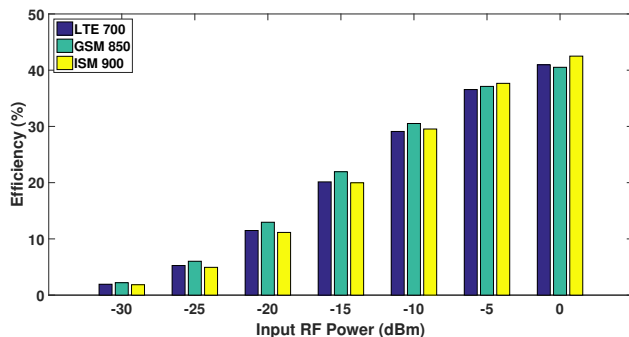
delivered to load and P_{RF} is the input RF power applied to the prototype.

$$P_{DC} = \frac{V_{Output}^2}{R_{Load}} \quad (2)$$

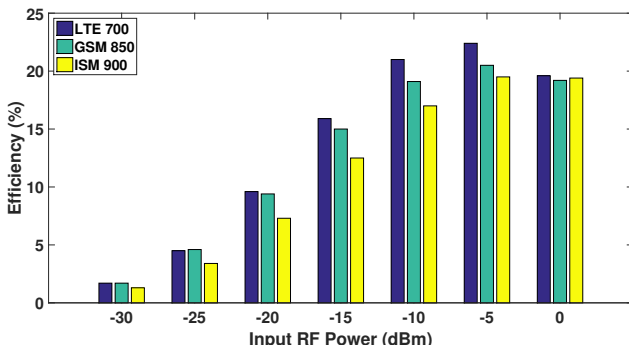
$$\eta = \frac{P_{DC}}{P_{RF}} \quad (3)$$



(a) PCE performance with 81KΩ Load for LTE 700, GSM 850, and ISM 900 bands



(b) PCE performance with 100KΩ Load for LTE 700, GSM 850, and ISM 900 bands



(c) PCE performance with 180KΩ Load for LTE 700, GSM 850, and ISM 900 bands

Fig. 23: Performance evaluation of our prototype at indoor environment.

Figure 23 shows that the proposed circuit obtains the highest PCE performance when RF input power range is between -10 and 0 dBm for LTE 700, GSM 850, and ISM 900 bands. As seen in Figure 7, the average available ambient RF power levels are in the same range as found in *MFA*, *Ell Hall*,

Symphony, and *Boston Common* in our city-wide study. This indicates that our circuit will power up the TI eZ430–RF2500 with high PCE performance for all determined bands at these locations. Additionally, our circuit can perform better than our previous ISM-only harvesting circuit reported in [10] in the low power regime (the input RF power range between -20 and 0 dBm) within the ISM 900 band. Even though our previously developed circuit only performs with the PCE range between 2% and 20%, our currently advanced design obtains the PCE range between 11% and 42% as seen in Figure 23b. This means that we enhance the performance of RF energy harvesting at ISM 900 Band with 100% improvement on PCE compared to our own previous effort.

Additionally, our circuit runs low-power micro-controllers (μ CUs) indoors with the input RF power range between -30 and -10 dBm in LTE and GSM bands. For instance, Texas Instruments' MSP430L092 consumes the power of 5.4μ W, 2.7μ W, and 40.5μ W in standby mode, LPM4 mode, and active mode respectively [25]. Our circuit supplies more than 6μ W DC power at input power ranges between -15 and -10 dBm, and 40μ W DC power at input power ranges between -10 and -5 dBm in LTE, GSM, and ISM bands. Therefore, our circuit can be used to power MSP430L092 in standby and LPM4 mode at as low as -15 dBm, and in active mode of MSP430L092, at as low as -10 dBm received RF power.

We further evaluate the application of our design in other WSN applications such as trigger charging, energy neutral, and radio wake-up operations [26]. For example, MSP430G2553 consumes 100nA with operation voltage of 1.8V in LPM4 mode, which translates to 180 nW [28]. Our prototype obtains 5% and 12% efficiency at -25 and -20 dBm, which are 158nW and 1.2μ W respectively. This means that it can run MSP430G2553 in LPM4 mode for trigger charging application at RF power range between -25 and -20 dBm, and sustain the energy neutral state of MSP430G2553 in LPM4 at less than 20 dBm in both LTE, GSM and ISM bands.

B. Outdoor Experimental Study

Figure 24 shows the ambient RF-EH system setup used in outdoor environment and battery-free communications. We use 6 dBi Ettus Research 50-ohm LP0410 Log Periodic PBC antenna [29] connected to the prototype. The prototype can run the sensor directly by delivering energy from the capacitor. We deploy two TI eZ430–RF2500 sensor motes including a ultra-low power micro-controller TI MSP430F2274 and a 2.4 GHz CC2500 radio chip. One is configured as the master sink, and the other that act as a slave that broadcasts ambient temperatures and battery voltage levels. The slave is connected to ambient RF-EH circuit.

The measurements are taken in six different locations as described in Section III and the output voltage is monitored when sensor node is not connected to the capacitor. The main task that allows sensor node to transmit data packets can only run when the capacitor has sufficient amount of voltage, which is 3.6 V for a sensor to turn on itself. The capacitor voltage must remain between 1.8 V and 3.6 V to run sensor operations after powering it up. The charging time is a key parameter,



Fig. 24: Battery-free communications setup for performance evaluation at outdoor environment.

defined as the time to charge the capacitor to the maximum desired voltage.

The RF charging time is measured at six locations for the LTE and GSM frequency bands, and compared to evaluate performance of our energy harvesting circuit. Figure 25 gives the cumulative distribution function (CDF) and probability distribution function (PDF) of RF charging times obtained from measurements where minimum and maximum voltage required

for the sensor operation is between 1.8 V and 3.6 V. We recall that a constant or stable RF source is a key parameter effecting the charging time of a capacitor, as seen from Figure 25a-25b. Thus, the stable power level (i.e. 110s) at *Ell Hall* provides fast charging compared to the locations such as *MFA* where we have measured time-varying fluctuations in power levels. In these alternate locations, it takes longer time to charge a capacitor even if the average ambient RF power is high (see Table II). These non-intuitive experimental results also exhibit that two locations, *Prudential* and *Arlington*, cannot provide sufficient ambient energy to charge the capacitor to the desired voltage level that allows running the sensor node.

In order to show feasibility of battery-free communications, harvest-first and harvest-and-use-later approaches have been integrated with an duty-cycling mechanism [30]. We have also implemented these approaches in our ambient RF-EH design. A duty-cycling mechanism allows the storage of ambient RF energy in the capacitor by switching between its operational sleep and active modes. We program the sensor to periodically wake up and transmit sensed data, including temperature and voltage values, to the master sink and go back into the sleep state. This enables the storage element to quickly and repeatedly recharge itself. In the sleep mode, a sensor consumes current of $20 \mu\text{A}$. In the active mode, the sensor is programmed to turn on MCU and start data communications with the master node. Here, sensor is prevented from discharging the capacitor down to below 1.8 V and charging itself up to above 3.6 V to ensure that the sensor cannot enter a non-operational state. Since current consumption of the sensor is $45 \mu\text{A}$ during active mode, our prototype is capable of operating a TI eZ430-RF2500 sensor continuously in battery-less mode (or active mode) as well as it can harvest and store energy from ambient RF power source at the same time as shown Figure 26.

VI. CONCLUSION

In this paper, we showed the practicality of a battery-free communication system using ambient RF signals as the only source of power. To this end, we first conducted a systematic study of RF energy availability in the Boston city, and then discussed design and fabrication constraints that lead to an efficient circuit design. Our work indicated that more than 65% of determined locations at Boston have enough RF power density to perpetually operate TI eZ430-RF2500 sensor mote in battery-less operation mode. We designed and implemented an RF-EH prototype can constantly operate TI eZ430-RF2500 sensor at multiple city locations, with efficiencies of up to 45% in LTE 700, GSM 850, and ISM 900 bands. Moreover, our design can support low-power TI μCUs such as MSP430L092 and MSP430G2553 in different operation modes, for e.g., active, standby and LPM4 mode at input RF power ranges between -25 and -5 dBm. As future work, we plan to use our ambient RF-EH prototype as ID-based low-cost ambient RF wake-up receiver for sensors at various locations in Boston city.

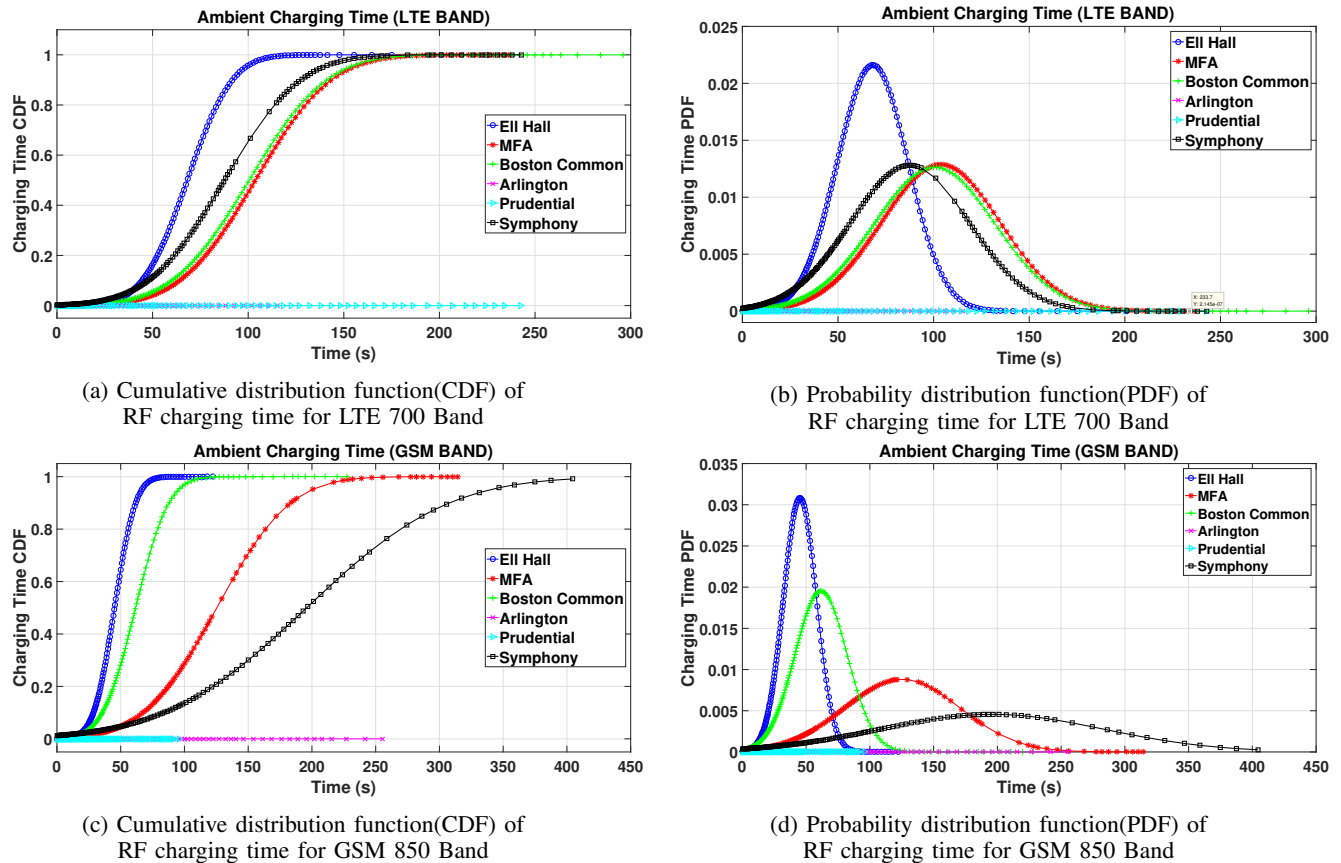


Fig. 25: Performance evaluations for outdoor experiments.

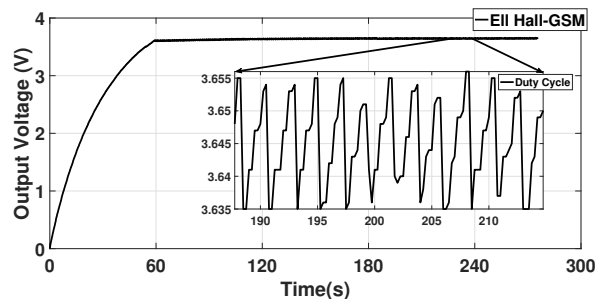


Fig. 26: Depicting charging and data communications cycles with capacitor voltage, when sensor node periodically wakes up during outdoor experiment.

VII. ACKNOWLEDGMENTS

We would like to thank Dr. M. Yousof Naderi for inputs on the RF spectrum survey and helpful feedback on the paper. This work is partially supported by the funds available through the US National Science Foundation award CNS 1452628.

REFERENCES

- [1] S. Keyrouz, H. J. Visser and A. G. Tjhuis, "Ambient RF energy harvesting from DTV stations," 2012 Loughborough Antennas & Propagation Conference (LAPC), Loughborough, 2012, pp. 1-4.
- [2] A. N. Parks and J. R. Smith, "Sifting through the airwaves: Efficient and scalable multiband RF harvesting," 2014 IEEE International Conference on RFID (IEEE RFID), Orlando, FL, 2014, pp. 74-81.
- [3] R. Margolies, M. Gorlatova, J. Sarik, G. Stanje, J. Zhu, P. Miller, M. Szczodrak, B. Vignham, L. Carloni, P. Kinget, I. Kymissis, and G. Zussman, "Energy-Harvesting Active Networked Tags (EnHANTs): Prototyping and Experimentation," *ACM Trans. Sen. Netw.* 11, 4, Article 62 (November 2015), 27 pages. DOI: <https://doi.org/10.1145/2831236>
- [4] L. Shuguang, J. Yuan, and H. Lipson, "Ambient wind energy harvesting using cross-flow fluttering," *Journal of Applied Physics* 109, 026104 (2011).
- [5] A. Cammarano, C. Petrioli and D. Spenza, "Pro-Energy: A novel energy prediction model for solar and wind energy-harvesting wireless sensor networks," 2012 IEEE 9th International Conference on Mobile Ad-Hoc and Sensor Systems (MASS 2012), Las Vegas, NV, 2012, pp. 75-83.
- [6] Y. K. Tan and S. K. Panda, "Optimized Wind Energy Harvesting System Using Resistance Emulator and Active Rectifier for Wireless Sensor Nodes," in *IEEE Transactions on Power Electronics*, vol. 26, no. 1, pp. 38-50, Jan. 2011.
- [7] J. Park, S. Han and T. Itoh, "A rectenna design with harmonic-rejecting circular-sector antenna," in *IEEE Antennas and Wireless Propagation Letters*, vol. 3, no. 1, pp. 52-54, Dec. 2004.
- [8] S. Scorcioni, L. Larcher, A. Bertacchini, L. Vincetti and M. Maini, "An integrated RF energy harvester for UHF wireless powering applications," 2013 IEEE Wireless Power Transfer (WPT), Perugia, 2013, pp. 92-95.
- [9] T. Le, K. Mayaram and T. Fiez, "Efficient Far-Field Radio Frequency Energy Harvesting for Passively Powered Sensor Networks," in *IEEE Journal of Solid-State Circuits*, vol. 43, no. 5, pp. 1287-1302, May 2008.
- [10] P. Nintanavongsa, U. Muncuk, D. R. Lewis and K. R. Chowdhury, "Design Optimization and Implementation for RF Energy Harvesting Circuits," in *IEEE Journal on Emerging and Selected Topics in Circuits and Systems*, vol. 2, no. 1, pp. 24-33, March 2012.
- [11] Z. Liu, Z. Zhong and Y. X. Guo, "Enhanced Dual-Band Ambient RF Energy Harvesting With Ultra-Wide Power Range," in *IEEE Microwave and Wireless Components Letters*, vol. 25, no. 9, pp. 630-632, Sept. 2015.
- [12] H. Nishimoto, Y. Kawahara and T. Asami, "Prototype implementation of ambient RF energy harvesting wireless sensor networks," 2010 IEEE Sensors, Kona, HI, 2010, pp. 1282-1287.

- [13] R. J. Vyas, B. B. Cook, Y. Kawahara and M. M. Tentzeris, "E-WEHP: A Batteryless Embedded Sensor-Platform Wirelessly Powered From Ambient Digital-TV Signals," in *IEEE Transactions on Microwave Theory and Techniques*, vol. 61, no. 6, pp. 2491-2505, June 2013.
- [14] R. Shigeta et al., "Ambient RF Energy Harvesting Sensor Device With Capacitor-Leakage-Aware Duty Cycle Control," in *IEEE Sensors Journal*, vol. 13, no. 8, pp. 2973-2983, Aug. 2013.
- [15] A. N. Parks, A. P. Sample, Y. Zhao and J. R. Smith, "A wireless sensing platform utilizing ambient RF energy," 2013 IEEE Topical Conference on Power Amplifiers for Wireless and Radio Applications, Santa Clara, CA, 2013, pp. 160-162
- [16] S. Keyrouz, H. J. Visser and A. G. Tijhuis, "Multi-band simultaneous radio frequency energy harvesting," 2013 7th European Conference on Antennas and Propagation (EuCAP), Gothenburg, 2013, pp. 3058-3061.
- [17] P2110B Series 850-950 MHz Power Harvester Development Kit Powercast Corp. [Online]. Available: <http://www.powercastco.com/products/development-kits/>
- [18] D. Masotti, A. Costanzo, M. D. Prete and V. Rizzoli, "Genetic-based design of a tetra-band high-efficiency radio-frequency energy harvesting system," in *IET Microwaves, Antennas & Propagation*, vol. 7, no. 15, pp. 1254-1263, December 10 2013.
- [19] M. Pinuea, P. D. Mitcheson and S. Lucyszyn, "Ambient RF Energy Harvesting in Urban and Semi-Urban Environments," in *IEEE Transactions on Microwave Theory and Techniques*, vol. 61, no. 7, pp. 2715-2726, July 2013.
- [20] A. N. Parks and J. R. Smith, "Active power summation for efficient multiband RF energy harvesting," 2015 IEEE MTT-S International Microwave Symposium, Phoenix, AZ, 2015, pp. 1-4.
- [21] M. Stoopman, S. Keyrouz, H. J. Visser, K. Philips and W. A. Serdijn, "Co-Design of a CMOS Rectifier and Small Loop Antenna for Highly Sensitive RF Energy Harvesters," in *IEEE Journal of Solid-State Circuits*, vol. 49, no. 3, pp. 622-634, March 2014.
- [22] S. Agrawal, S. K. Pandey, J. Singh and M. S. Parihar, "Realization of efficient RF energy harvesting circuits employing different matching technique," Fifteenth International Symposium on Quality Electronic Design, Santa Clara, CA, 2014, pp. 754-761.
- [23] S. D. Assimonis, S. N. Daskalakis and A. Bletsas, "Sensitive and Efficient RF Harvesting Supply for Batteryless Backscatter Networks," in *IEEE Transactions on Microwave Theory and Techniques*, vol. 64, no. 4, pp. 1327-1338, April 2016.
- [24] U. Muncuk, "Design optimization and implementation for RF energy harvesting circuits," Master of Science Thesis, Northeastern University, Boston, USA, 2012.
- [25] Texas Instruments MSP430L092, [Online]. Available: <http://www.ti.com/product/msp430l092>
- [26] L. Chen, S. Cool, H. Ba, W. Heinzelman, I. Demirkol, U. Muncuk, K. Chowdhury, and S. Basagni, "Range extension of passive wake-up radio systems through energy harvesting," 2013 IEEE International Conference on Communications (ICC), Budapest, 2013, pp. 1549-1554.
- [27] D. W. Harrist, "Wireless Battery Charging System Using Radio Frequency Energy Harvesting", *Master of Science Thesis*, University of Pittsburgh, USA, 2004.
- [28] Texas Instruments, MSP430G2553 [Online]. Available: <http://www.ti.com/product/MSP430G2553>
- [29] LP0410 Log Periodic PCB Antenna (400 MHz to 1 GHz) Wideband [Online]. Available: <https://www.ettus.com/product/details/LP0410>
- [30] S. Peng, C.P. Low, "Prediction free energy neutral power management for energy harvesting wireless sensor nodes," *Ad Hoc Networks*, Volume 13, Part B, February 2014, Pages 351-367, ISSN 1570-8705



Ufuk Muncuk received the B.S. degree in Electrical and Electronics Engineering from Firat University, Elazig, Turkey, in 2008, and the M.S. degree in Electrical and Electronics Engineering from Erziyes University, Kayseri, Turkey, in 2009 and M.S. degree in Computer Engineering from Northeastern University, Boston, MA, in 2012, respectively. He started the Ph.D. degree in Computer Engineering at Northeastern University, Boston, MA in 2012.

His research interests include Design, Optimization and Implementation for RF Energy Harvesting Circuits, Use of Wireless Energy Transfer, System Design for Joint RF Energy and Magnetic Coupling-Based Energy Transfer, System design for intra-body transceivers. Analog and Digital Circuit Design, Wireless Sensor Networks, Cognitive Radio Systems



Kubra Alemdar received B.S degree in Electrical and Electronics Engineering in 2011 and B.S degree in Computer Engineering in 2012 from Fatih University, Istanbul, Turkey. She received a M.S Degree in Electrical and Electronics Engineering from Fatih University in 2014, on the Scientific Technological Research Council of Turkey (TUBITAK) scholarship. She started the Ph.D degree in electrical and computer engineering at Northeastern University, Boston, MA, in 2015. Her research interests are wireless power transfer and RF energy harvesting.



Jayesh D. Sarode received his B.S degree in Electronics and Communication in 2013 and M.S degree in Chemistry in 2013 at BITS Pilani in India. He is specializing with focus on computer architecture, networking and embedded systems. He is presently working on research project titled as "Integrated Data and Energy Access for Wireless Sensor Networks" at Genesys lab in Northeastern University. He is also doing internship at Bose Corporation in Professional Music Systems division. He has worked with multiple companies in the past like Broadcom,

Tatvik and eGain Communication.



Kaushik Roy Chowdhury (M09-SM15) received the M.S. degree from the University of Cincinnati in 2006, and the Ph.D. degree from the Georgia Institute of Technology in 2009. He was an Assistant Professor from 2009 to 2015 at Northeastern University, where he is currently an Associate Professor with the Electrical and Computer Engineering Department. Prof. Chowdhury is the winner of the U.S. Presidential Early Career Award for Scientists and Engineers (PECASE) in 2017, the Defense Advanced Research Projects Agency Young Faculty

Award in 2017, the Office of Naval Research Director of Research Early Career Award in 2016, and the National Science Foundation (NSF) CAREER award in 2015.